

# Effect of Alkyl Chain Length on Adsorption Behavior and Corrosion Inhibition of Imidazoline Inhibitors

**Jafari, Hojat\***<sup>†•</sup>

*Abadan Faculty of Petroleum Engineering, Petroleum University of Technology, Abadan, I.R. IRAN*

**Mohsenifar, Farhad**

*Department of Mechanical Engineering, Higher Education Complex of Bam, Bam, I.R. IRAN*

**Sayin, Koray**

*Department of Chemistry, Institute of Science, Cumhuriyet University, 58140 Sivas, TURKEY*

**ABSTRACT:** *Inhibition performances of imidazoline derivatives with different alkyl chain length for carbon steel in H<sub>2</sub>S acid solutions has been studied by polarization curves, AC impedance measurements, current transient, Atomic Force Microscopy (AFM) and Density functional theory (DFT) techniques. Results showed that the inhibition occurs through adsorption of the inhibitors molecules on the metal surface. The inhibition efficiency was found to increase with increasing inhibitor's concentration. Polarization data indicated that this compounds act as mixed-type inhibitors. Computational studies of investigated inhibitors were performed by using Hartree–Fock (HF) and M062X methods which are ab-initio and DFT methods with 6-31G basis set in gas phase and water. Calculated results indicate that the inferred inhibition efficiency increases with the increasing alkyl chain length, which is well in accordance with reported experimental results.*

**KEYWORDS:** *Metals; Organic compounds; Ab initio calculations; Corrosion; Computer modelling and simulation.*

## INTRODUCTION

Corrosion is brought about by environmental factors such as humidity, acid rain etc. and results in damages to materials during their useful life. *Feng et al.* (2003) reported that a higher humidity of the air resulted in an increased corrosion rate of steel [1]. According to a US study, 4.9% of the GNP of industrialized nations has been attributed to direct costs of corrosion [2]. Corrosion may then lead to other costs such as loss of efficiency,

contamination and power failures. In addition, it is also estimated that 40% of the steel produced is used for replacement of corroded steel [3].

In most cases, high aggressiveness of operated environments (natural and associated petroleum gases, oil, and hydrocarbon condensate) is caused moisture and sour components, such as H<sub>2</sub>S [4, 5], where H<sub>2</sub>S is especially dangerous because it stimulates corrosion and

---

\* To whom correspondence should be addressed.

+ E-mail: [hojatjafari80@yahoo.com](mailto:hojatjafari80@yahoo.com)

• Other Address: *Iranian Offshore Oil Company, National Iranian Oil Company, Lavan, I.R. IRAN*  
1021-9986/2018/5/85-103 19/\$/6.09

accelerates hydrogenation which leads to the loss of plasticity properties of steel and cracking [5].

The use of inhibitors is one of the most practical methods for protection against corrosion, especially in acidic media. Among numerous inhibitors that have been tested and applied industrially as corrosion inhibitors, those that are nontoxic or of low toxicity are now far more strategic than in the recent past. In the twenty first century, research in the field of “green” or “eco-friendly” corrosion inhibitors have been addressed toward the goal of using cheap, effective compounds of low or “zero” environmental impact. Organic compounds bearing heteroatoms with high electron density such as phosphor, sulphur, nitrogen, oxygen or those containing multiple bonds which are considered as adsorption centers, are effective as corrosion inhibitor [6-11]. The compounds contain both nitrogen and sulphur in their molecular structure has exhibited greater inhibition compared with those contain only one of these atoms [11–14].

Among various types of corrosion inhibitors, imidazoline derivatives have been proved to be effective in controlling corrosion [6-8]. The molecular structure of imidazoline consists of three parts: a five-atom ring with two nitrogen atoms, a pendant side chain as a hydrophilic group and a long hydrocarbon chain as a hydrophobic group. It is well accepted that the substitutional group attached to the five-atom ring has a great effect on the inhibition performance of the inhibitor [7,8].

Wang *et al.* [6] studied the inhibition performance of a thioureido imidazoline inhibitor in CO<sub>2</sub>-saturated solution. Results show that it can efficiently inhibit Q235 steel from CO<sub>2</sub> corrosion, and the inhibition efficiency shows a peak-value-phenomenon at a concentration of 0.15 mmol/L as a result of the change in adsorption mode. Liu *et al.* [7] studied the electrochemical behavior of carbon steel in CO<sub>2</sub>-saturated saltwater with and without a new synthesized imidazoline inhibitor. Those results show that the imidazoline is a kind of mixed-type inhibitor and its adsorption on Q235 steel fits Frumkin isotherm equation. Zheng *et al.* [8] studied the inhibition performances of 2-undecyl-1-aminoethyl imidazoline (AEI-11) and 2-undecyl-1-aminoethyl-1-hydroxyethyl quaternary imidazoline (AQI-11) on CO<sub>2</sub> corrosion of N80 mild steel in single liquid phase and liquid/particle two-phase flow. The results show that AQI-11 exhibits

better inhibition ability than AEI-11 in both phases due to the polycentric adsorption sites on its structure.

Quantum chemical calculations is a very powerful technique to probe the inhibitor/surface interaction and to analyze experimental data [9,11]. These are the reasons why we selected both electrochemical and quantum chemical methods to evaluate the efficiency of inhibitors.

The objective of this work is to present the relationships between the imidazoline derivative reactivity and their ability to inhibit the corrosion of steel in H<sub>2</sub>S. To understand if any structural differences induced by different alkyl chain length may be related to the experimentally observed differences of corrosion efficiency.

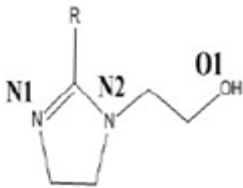
Computational studies of six corrosion inhibitors (Fig.1) are done by using HF/6-31G and M062X/6-31G levels in gas phase and water. A new formula for investigated inhibitors and their derivatives is derivate by matrix solution.

## EXPERIMENTAL SECTION

50 steel samples were cut from parent pipe with chemical composition reported as C: 0.07, Si: 0.0032, P: 0.08, S: 0.002, Mn: 0.034%w, Fe: Rest. The aggressive solution of H<sub>2</sub>S with pH = 4 was prepared by dilution of Merck Product H<sub>2</sub>S. All chemicals used in the present work were of reagent-grade Merck products were used as-received without further purification. The inhibitors (Fig. 1) were synthesized with the raw materials [12] of diethylenetriamine, benzoic acid and benzyl chloride at different molar ratios. according to the described procedure by Anastas (2014) [12].

The apparatus for electrochemical investigations consists of a computer-controlled Auto Lab potentiostat/galvanostat (PGSTAT302N) corrosion measurement system at a scan rate of 1mV/s. The experiments were carried out using a conventional three electrode cell assembly at 25 ± 2 °C. A rectangular platinum foil was used as counter electrode and saturated calomel electrode as the reference electrode. Time interval of 25-30 min was given for steady-state attainment of open circuit potential. The EIS experiments were conducted in the frequency range of 100 kHz to 0.01 Hz at open circuit potential. The AC potential amplitude was 10 mV.

For surface analysis, the specimens of size 0.32 cm<sup>2</sup> were abraded with Emery paper (up to 1200) to give

Molecular structure	R	Name	Abbr.
	$-\text{CH}_2(\text{CH}_2)_5\text{CH}_3$	1-(2-hydroxyethyl)-2-heptyl-imidazole	Inhibitor (1)
	$-\text{CH}_2(\text{CH}_2)_7\text{CH}_3$	1-(2-hydroxyethyl)-2-heptyl-imidazole	Inhibitor (2)
	$-\text{CH}_2(\text{CH}_2)_9\text{CH}_3$	1-(2-hydroxyethyl)-2-heptyl-imidazole	Inhibitor (3)
	$-\text{CH}_2(\text{CH}_2)_{11}\text{CH}_3$	1-(2-hydroxyethyl)-2-heptyl-imidazole	Inhibitor (4)
	$-\text{CH}_2(\text{CH}_2)_{13}\text{CH}_3$	1-(2-hydroxyethyl)-2-heptyl-imidazole	Inhibitor (5)
	$-\text{CH}_2(\text{CH}_2)_{15}\text{CH}_3$	1-(2-hydroxyethyl)-2-heptyl-imidazole	Inhibitor (6)

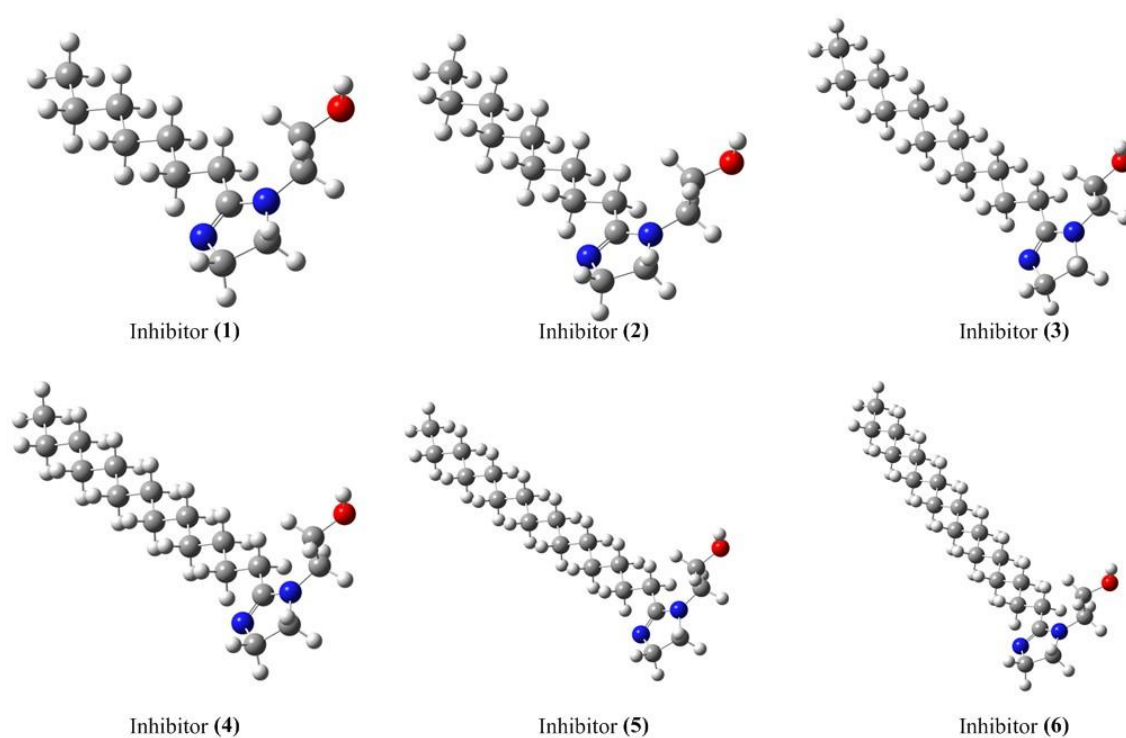


**Fig. 1:** Schematic representation of inhibitors and Optimized structures of mentioned inhibitors at HF/6-31G level in water.

a homogeneous surface, then washed with distilled water and acetone. The specimens were immersed in  $\text{H}_2\text{S}$  prepared with and without addition of  $2 \times 10^{-3}$  M inhibitors at  $25^\circ\text{C}$  for 24 h, cleaned with distilled water. The surface morphology of the electrode surface was evaluated by Atomic Force Microscopy (AFM) Nan Surf easy scan 2.

All progresses on computer were done by using GaussView 5.0.8 [13], Gaussian 09 AM64L-G09RevD.01 package programme [14], ChemBioDraw

Ultra Version (13.0.0.3015) [15]. HF method was selected as computational method for our inhibitors. In calculations, 6-31G was selected as basis set. All calculations were performed in gas phase and water. The vibration frequency analyses showed that the optimized structures of all inhibitors are at stationary points corresponding to local minima without imaginary frequencies. The interactions of solute solvent were taken into account by the conductor-like polarizable continuum model (PCM). Some quantum chemical descriptors were

calculated by using Eq. (1) – (12) [16 – 28]. For a system of  $N$  electrons, independent single point calculation is performed, at the same level of theory, for corresponding  $N + 1$  and  $N - 1$  electron system. The natural population analysis yields to  $P_k(N - 1)$ ,  $P_k(N)$  and  $P_k(N + 1)$ ; the population for all  $k$  atoms.

$$E_{CAP} = E_{LUMO} - E_{HOMO} \quad (1)$$

$$I = -E_{HOMO} \quad (2)$$

$$A = -E_{LUMO} \quad (3)$$

$$\eta = \frac{|I - A|}{2} \quad (4)$$

$$\sigma = \frac{1}{\eta} \quad (5)$$

$$\chi = \frac{|E_{HOMO} + E_{LUMO}|}{2} \quad (6)$$

$$\mu = -\chi \quad (7)$$

$$\omega = \frac{\mu^2}{2\eta} \quad (8)$$

$$N = \frac{1}{\omega} \quad (9)$$

$$f_k^+ = P_k(N+1) - P_k(N) \quad (10)$$

$$f_k^- = P_k(N) - P_k(N-1) \quad (11)$$

$$f_k^0 = \frac{P_k(N+1) - P_k(N-1)}{2} \quad (12)$$

$$\Delta H_{H^+} = \Delta H_{H_3O^+} - \Delta H_{H_2O} \quad (13)$$

$$PA = \Delta H_{pro.inh.} - (\Delta H_{non-pro.inh.} + \Delta H_{H^+}) \quad (14)$$

$$E_{int.} = E_{complex} - (E_{inhibitor} + E_{Metal}) \quad (15)$$

Where  $E_{HOMO}$  and  $E_{LUMO}$  are the energy of the Frontier molecular orbital HOMO and LUMO. The ionization potential ( $I$ ), the electron affinity ( $A$ ), electronegativity ( $\chi$ ), chemical potential ( $\mu$ ), hardness ( $\eta$ ), softness ( $\sigma$ ), electrophilicity index ( $\omega$ ) and Nucleophilicity index ( $N$ ) are given by Eqs. (2)–(9). The Fukui function is  $f$  and  $P_k(N)$ ,  $P_k(N+1)$ ,  $P_k(N-1)$  are the electron population of

the  $k^{th}$  atom for  $N$ ,  $N+1$ , and  $N-1$  electron systems, respectively.  $\Delta H^+$ ,  $\Delta H_{H_3O^+}$ ,  $\Delta H_{H_2O}$ ,  $\Delta H_{pro.inh.}$ ,  $\Delta H_{non-pro.inh.}$ ,  $PA$ ,  $E_{int.}$ ,  $E_{complex}$ ,  $E_{inhibitor}$  and  $E_{metal}$  are enthalpy of proton, enthalpy of hydronium, enthalpy of water, enthalpy of protonated inhibitor, enthalpy of non-protonated inhibitor, proton affinity, interaction energy, total energy of complex, total energy of inhibitor and total energy of metal atom, respectively.

## RESULTS AND DISCUSSION

### Electrochemical results

Polarization curves were obtained for steel in acidic solution with and without inhibitors. Tafel lines which were obtained in  $2 \times 10^{-3}$  M of imidazoline derivative with different alkyl chain length in acidic solutions were shown in Fig.2, at 25°C respectively. The corresponding electrochemical parameters, i.e., corrosion potential ( $E_{corr}$  versus SCE), corrosion current density ( $I_{corr}$ ), cathodic and anodic Tafel slopes ( $\beta_a$ ,  $\beta_c$ ) and the degree of surface coverage ( $\theta$ ) values were calculated from these curves and are given in Table 1.

The degree of surface coverage for different inhibitors is calculated using the following equations [29, 30]:

$$\theta = \frac{I - \dot{I}}{I} \quad (16)$$

Where  $I$  and  $\dot{I}$  are the corrosion current densities without and with corrosion inhibitor, respectively, determined by the intersection of the extrapolated Tafel lines at the corrosion potential for steel in uninhibited and inhibited acid solution. The presence of imidazoline derivatives shifts both anodic and cathodic branches to the lower values of current densities and thus causes a remarkable decrease in the corrosion rate. It can be clearly seen from Fig. 2 that both anodic metal dissolution of iron and cathodic hydrogen evolution reactions were inhibited after the addition of inhibitors to the aggressive solution. This result is indicative of the adsorption of inhibitor molecules on the active sites of steel surface [31]. The inhibition of both anodic and cathodic reactions is more pronounced with the increasing alkyl chain length. However, the influence is more pronounced in the cathodic polarization plots compared to that of the anodic polarization plots. The cathodic current–potential curves (Fig. 2) giving rise to parallel lines indicates that the addition of inhibitors to the solution does not modify

**Table 1: Potentiodynamic polarization parameters for the corrosion of steel in acidic solution in absence and in the presence of imidazoline derivatives with different alkyl chain length at 25 °C.**

Inhibitor	$-E_{corr}$ , mV	$I_{corr}$ , $\mu\text{A}/\text{cm}^2$	$\beta_a$ , mV/dec	$-\beta_c$ , mV/dec	$R_p$ , $\Omega \text{ cm}^2$	$\theta$
blank	509	327	79	110	251	----
Inhibitor (1)	495	219	71	118	355	0.33
Inhibitor (2)	490	181	68	105	464	0.45
Inhibitor (3)	487	148	85	125	788	0.54
Inhibitor (4)	483	101	87	129	1133	0.69
Inhibitor (5)	478	37	79	101	4230	0.88
Inhibitor (6)	470	13	80	125	7572	0.96

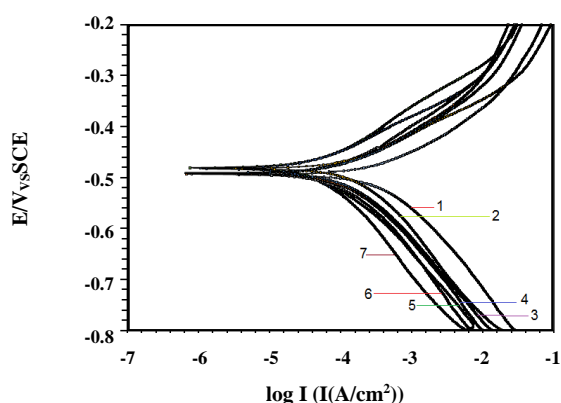


**Fig. 2: Anodic and cathodic polarization curves for steel in acidic solution without and with  $2 \times 10^{-3}$  M of investigated inhibitors at 25 °C: 1.blank, 2. Inhibitor (1), 3. Inhibitor (2), 4. Inhibitor (3), 5. Inhibitor (4), 6. Inhibitor (5), 7. Inhibitor (6).**

the reduction mechanism and the reduction at steel surface takes place mainly through a charge transfer mechanism [31-34]. The slopes do not display an order with the inhibitor concentration; this feature indicates that inhibition occurred by a blocking mechanism on the available metal spaces [35-38]. The corrosion potential displayed small change in the range of  $-470$  to  $-509$  mV vs. SCE and curves changed slightly towards the positive direction (Fig. 2).

These results indicated that the presence of compounds inhibited iron oxidation and in a lower extent hydrogen evolution, consequently these compounds can be classified as mixed corrosion inhibitors, as electrode potential displacement is lower than 85 mV in any direction [39]. The polarization resistance ( $R_p$ ) from Tafel extrapolation method was calculated using the Stern–Geary Equation (Eq.17) [40].

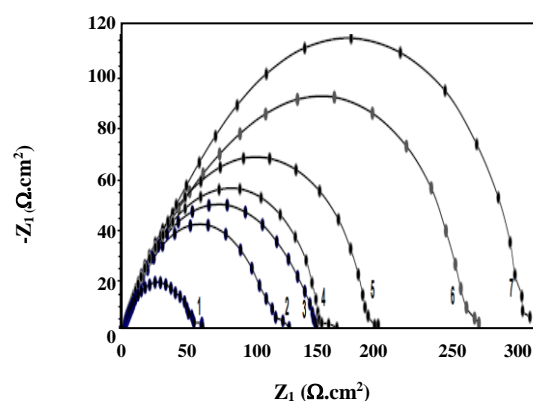


**Fig. 3: Nyquist plots for steel in acidic solution without and with  $2 \times 10^{-3}$  M of investigated inhibitors at 25 °C: 1.blank, 2. Inhibitor (1), 3. Inhibitor (2), 4. Inhibitor (3), 5. Inhibitor (4), 6. Inhibitor (5), 7. Inhibitor (6).**

$$R_p = \frac{\beta_a \cdot \beta_c}{2.303(\beta_a + \beta_c)} \times \frac{1}{I_{corr}} \quad (17)$$

By increasing the inhibitor alkyl chain length, the polarization resistance increases in the presence of the compound, indicating adsorption of the inhibitor on the metal surface to block the active sites efficiently and inhibit corrosion [41].

Fig. 3 shows the Nyquist diagrams of steel in acidic solutions containing different concentrations of imidazoline derivatives at 25 °C respectively. All the impedance spectra exhibit single depressed semicircle. The diameter of semicircle increases with the increase of alkyl chain length. The semicircular appearance shows that the corrosion of steel is controlled by the charge transfer and the presence of imidazoline derivatives does not change the mechanism of steel dissolution [42,43].

In addition, these Nyquist diagrams are not perfect semicircles. The deviation of semicircles from perfect circular shape is often referred to the frequency dispersion of interfacial impedance [43-46]. This behaviour is usually attributed to the inhomogeneity of the metal surface arising from surface roughness or interfacial phenomena [41,42], which is typical for solid metal electrodes [47].

The equivalent circuit compatible with the Nyquist diagram recorded in the presence of inhibitor is depicted in Fig. 4.a. The simplest approach requires the theoretical transfer function  $Z(\omega)$  to be represented by a parallel combination of a resistance  $R_{ct}$  and a capacitance  $C$ , both in series with another resistance  $R_s$  [48].

$$Z(\omega) = R_s + \frac{1}{\frac{1}{R_{ct}} + i\omega C} \quad (18)$$

Where  $\omega$  is the frequency in rad/s,  $\omega = 2\pi f$  and  $f$  is frequency in Hz. To obtain a satisfactory impedance simulation of steel, it is necessary to replace the Capacitor (C) with a Constant Phase Element (CPE)  $Q$  in the equivalent circuit. The most widely accepted explanation for the presence of CPE behavior and depressed semicircles on solid electrodes is microscopic roughness, causing an inhomogeneous distribution in the solution resistance as well as in the double layer capacitance [48].  $Q_{dl}$ ,  $R_s$  and  $R_{ct}$  can be corresponded to double layer capacitance, solution resistance and charge transfer resistance, respectively.

Computer fitting of the spectrum allows evolution of the elements of the circuit analogue. The aim of the fitting procedure is to find those values of the parameters which best describe the data, i.e., the fitting model must be consistent with the experimental data. To corroborate the equivalent circuit, the experimental data are fitted to equivalent circuit (Fig.4.a and 4.b) and the circuit elements are obtained. Table 2 illustrates the equivalent circuit parameters for the impedance spectra of corrosion of steel in acidic Solution. The data indicate that increasing charge transfer resistance is associated with a decrease in the double layer capacitance. It has been reported that the adsorption of organic inhibitor on the metal surface is characterized by a decrease in  $C_{dl}$  [3]. The decreased values of  $C_{dl}$  may be due to the replacement of water molecules at the electrode interface

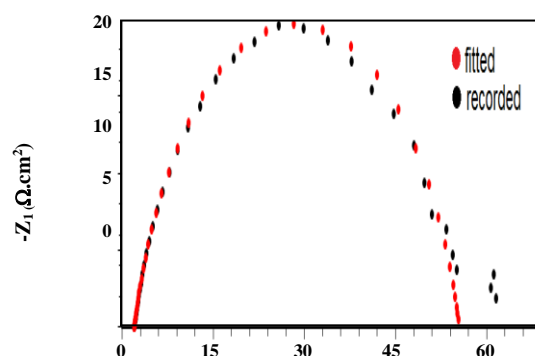
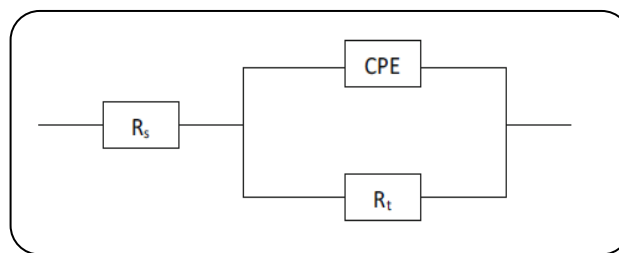


Fig. 4: a) Equivalent circuits compatible with the experimental impedance data in Fig 3. B) Experimental and computer fit result of Nyquist plot for steel in acidic solution at 25 °C.

by organic inhibitor of lower dielectric constant through adsorption, suggests that inhibitor acts by adsorption at the metal-solution interface. The increase in values of  $R_{ct}$  and the decrease in values of  $C_{dl}$  with increasing the alkyl chain length also indicate that imidazoline derivatives acts as primary interface inhibitor and the charge transfer controls the corrosion of steel under the open circuit conditions [40].

### Chronoamperometry

In order to gain more insight about the effect of inhibitor on the electrochemical behavior of steel in acidic solution, potentiostatic current-time transients were recorded. Fig 5 shows the current transients of steel electrode at -0.4 V versus SCE applied anodic potential.

As can be seen, in the absence of inhibitor, initially, the current decreases monotonically with time. The decrease in the current density is due to the formation of corrosion products layer on the anode surface. However, in later times the current reach a steady state value depending on applied potential. In the presence of inhibitor, change in current was not observed and

**Table 2: Impedance data for steel in acidic solution in absence and in the presence of imidazoline derivatives with different alkyl chain length at 25 °C.**

Inhibitor	$R_s, \Omega \text{ cm}^2$	$R_{ct}, \Omega \text{ cm}^2$	$Q_{dl}, \text{mF cm}^2$	n
blank	1.6	61	0.731	0.74
Inhibitor (1)	1.6	114	0.519	0.74
Inhibitor (2)	1.5	145	0.357	0.75
Inhibitor (3)	1.5	147	0.353	0.76
Inhibitor (4)	1.4	184	0.211	0.76
Inhibitor (5)	1.3	267	0.204	0.78
Inhibitor (6)	1.4	302	0.195	0.81

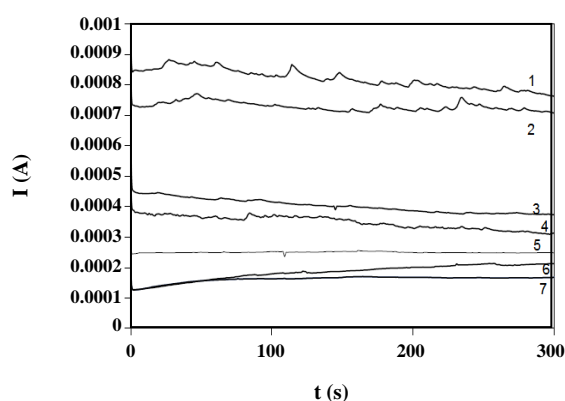


**Fig. 5: Current transients of steel electrode at -0.4 V vs. SCE: 1. blank, 2. Inhibitor (1), 3. Inhibitor (2), 4. Inhibitor (3), 5. Inhibitor (4), 6. Inhibitor (5), 7. Inhibitor (6).**

electrode was inhibited from corrosion due to inhibitor adsorption. If the current-time transients are decisive for investigated inhibitors, the ranking of the compounds should be:

$$\text{Inhibitor (6)} > \text{Inhibitor (5)} \approx \text{Inhibitor (4)} \approx \text{Inhibitor (3)} > \text{Inhibitor (2)} > \text{Inhibitor (1)}$$

### Surface photographs

The surface photographs of steel, which were immersed in blank and containing imidazoline derivative with different alkyl chain length after 24 h, were presented in Fig. 6. It can be seen clearly from Fig. 6 (2-7), that there is a good surface coverage on the steel surface in the presence of inhibitor which provides a good corrosion inhibition efficiency. This is due to the involvement of inhibitor molecules in the interaction with the reaction sites of steel surface, resulting in a decrease in the contact between iron and the aggressive medium and sequentially exhibited excellent inhibition effect.

It was observed that the sample in contact solution gave high corrosion attack (Fig.6.1), on the other hand, in the presence of imidazoline derivative with different alkyl chain length smooth surfaces were obtained, and the degree of attack decreased. This is in good agreement with the result obtained from the EIS tests that with the increasing of alkyl chain length in acidic solutions increase the exponent n of the double layer capacitance.

### Non-protonated inhibitors

Optimized structures of 1-(2-hydroxyethyl)-2-heptyl-imidazoline (1), 1-(2-hydroxyethyl)-2-heptyl-imidazoline (2), 1-(2-hydroxyethyl)-2-heptyl-imidazoline (3), 1-(2-hydroxyethyl)-2-heptyl-imidazoline (4), 1-(2-hydroxyethyl)-2-heptyl-imidazoline (5) and 1-(2-hydroxyethyl)-2-heptyl-imidazoline (6) are optimized at HF/6-31G and M062X/6-31G levels in gas phase and water and represented in Fig. 1 at HF/6-31G level in water. For non-protonated inhibitors, quantum chemical descriptors are calculated by using HF/6-31G and M062X/6-31G level in gas phase and water. Mentioned parameters are listed in Table 3.

$E_{\text{HOMO}}$  is the most commonly used quantum chemical parameter and mainly associated with electron donating ability of molecules. High value of HOMO energy implies the tendency of electron transfer to low unoccupied molecular orbital of appropriate acceptor molecule.

If the  $E_{\text{HOMO}}$  are decisive for investigated inhibitors, the ranking of the compounds should be:

$$\text{Inhibitor (6)} > \text{Inhibitor (5)} \approx \text{Inhibitor (4)} \approx \text{Inhibitor (3)} > \text{Inhibitor (2)} > \text{Inhibitor (1)}$$

The  $E_{\text{GAP}}$  is an important parameter as a function of activity of the corrosion inhibitors towards to metallic bulk. The smaller  $E_{\text{GAP}}$  values mean higher inhibition efficiency.

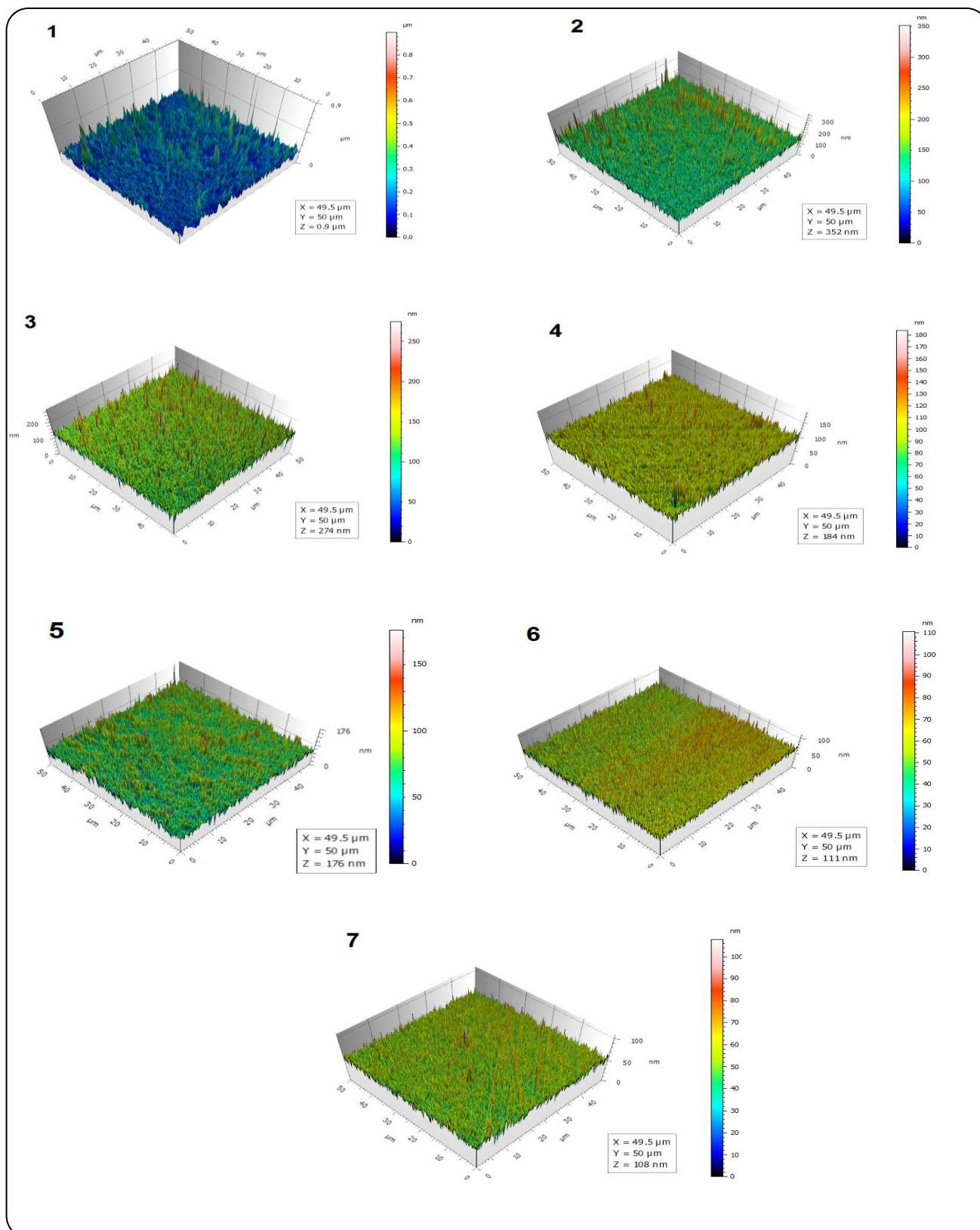


Fig. 6: AFM images of for steel in acidic solution without and with  $2 \times 10^{-3}$  M of investigated inhibitors: 1. blank, 2. Inhibitor (1), 3. Inhibitor (2), 4. Inhibitor (3), 5. Inhibitor (4), 6. Inhibitor (5), and 7. Inhibitor (6) (scansize:  $49.5 \times 50 \mu\text{m}$ ).



**Table 3: Quantum chemical descriptors for non-protonated inhibitors at HF/ 6-31G and M062X/6-31G levels in gas phase and water.**

Inhibitors	$E_{\text{HOMO}}^a$	$E_{\text{LUMO}}^a$	$E_{\text{GAP}}^a$	$\eta^a$	$\sigma^b$	$\chi^a$	$\omega^a$	$N^b$
HF/6-31G in gas phase								
Inhibitor (1)	-8.474	5.500	13.974	6.987	0.143	1.487	0.158	6.320
Inhibitor (2)	-8.473	5.501	13.974	6.987	0.143	1.486	0.158	6.327
Inhibitor (3)	-8.472	5.501	13.974	6.987	0.143	1.486	0.158	6.331
Inhibitor (4)	-8.472	5.502	13.974	6.987	0.143	1.485	0.158	6.335
Inhibitor (5)	-8.526	5.502	14.027	7.014	0.143	1.512	0.163	6.137
Inhibitor (6)	-8.472	5.502	13.974	6.987	0.143	1.485	0.158	6.337
HF/6-31G in water								
Inhibitor (1)	-8.593	5.349	13.942	6.971	0.143	1.622	0.189	5.300
Inhibitor (2)	-8.592	5.350	13.942	6.971	0.143	1.621	0.188	5.306
Inhibitor (3)	-8.591	5.350	13.942	6.971	0.143	1.620	0.188	5.310
Inhibitor (4)	-8.591	5.351	13.942	6.971	0.143	1.620	0.188	5.312
Inhibitor (5)	-8.591	5.351	13.942	6.971	0.143	1.620	0.188	5.314
Inhibitor (6)	-8.590	5.351	13.941	6.971	0.143	1.620	0.188	5.314
M062X/6-31G in gas phase								
Inhibitor (1)	-6.832	2.290	9.121	4.561	0.219	2.271	0.565	1.769
Inhibitor (2)	-6.833	2.287	9.120	4.560	0.219	2.273	0.566	1.766
Inhibitor (3)	-6.831	2.288	9.119	4.560	0.219	2.272	0.566	1.767
Inhibitor (4)	-6.829	2.289	9.118	4.559	0.219	2.270	0.565	1.770
Inhibitor (5)	-6.803	2.308	9.111	4.555	0.220	2.248	0.555	1.803
Inhibitor (6)	-6.798	2.311	9.109	4.555	0.220	2.244	0.553	1.810
M062X/6-31G in water								
Inhibitor (1)	-6.926	-2.124	4.802	2.401	0.416	4.525	4.263	0.235
Inhibitor (2)	-6.893	2.135	9.028	4.514	0.222	2.379	0.627	1.595
Inhibitor (3)	-6.894	2.134	9.028	4.514	0.222	2.380	0.628	1.593
Inhibitor (4)	-6.894	2.133	9.028	4.514	0.222	2.381	0.628	1.593
Inhibitor (5)	-6.894	2.133	9.028	4.514	0.222	2.381	0.628	1.593
Inhibitor (6)	-6.894	2.134	9.028	4.514	0.222	2.380	0.628	1.593

<sup>a</sup> in eV, <sup>b</sup> in eV<sup>-1</sup>

According to  $E_{\text{GAP}}$  values, the ranking of inhibition efficiency should be as follows:

Inhibitor (6) > Inhibitor (5)  $\approx$  Inhibitor (4)  $\approx$  Inhibitor (3)  $\approx$  Inhibitor (2)  $\approx$  Inhibitor (1)

Other important parameters are hardness ( $\eta$ ) and softness ( $\sigma$ ) to explain the inhibitors efficiencies. Tendencies of electron transferring of inhibitors towards metal surface can be discussed with Hard-Soft-Acid-Base (HSAB) approximation [28]. According to this approximation, hard/soft chemical species prefer to coordinate to hard/soft species. Consequently, soft species are to be most effective for metallic bulks. Since, metallic bulk is softer than metal atoms. According to softness values, inhibition efficiency ranking should be:

Inhibitor (6) > Inhibitor (5)  $\approx$  Inhibitor (4)  $\approx$  Inhibitor (3)  $\approx$  Inhibitor (2)  $\approx$  Inhibitor (1)

Other important parameter is absolute electronegativity. The electronegativity is related with freedom electron mobility in inhibitor molecule. Corrosion inhibitors coordinate to metal surface by giving electrons. The inhibition efficiency therefore increases with decreasing of absolute electronegativity values. According to absolute electronegativity, inhibition efficiency ranking should be as follow:

Inhibitor (6)  $\approx$  Inhibitor (5)  $\approx$  Inhibitor (4)  $\approx$  Inhibitor (3) > Inhibitor (2) > Inhibitor (1)

The electrophilicity index ( $\omega$ ) implies the ability of the inhibitor molecules to accept electrons and nucleophilicity index ( $N$ ) displays the ability of inhibitors to donate electrons which are used as quantum chemical parameters. The inhibition efficiency increases with increasing the  $N$  value or decreasing the  $\omega$  value. According to the  $N$  and  $\omega$ , theoretical inhibition efficiency ranking should be:

Inhibitor (6)  $\approx$  Inhibitor (5)  $\approx$  Inhibitor (4)  $\approx$  Inhibitor (3) > Inhibitor (2) > Inhibitor (1)

As a result, there is an agreement between experimental and calculated results. HF/6-31G level in water is taken into account for other calculations.

#### Determination of active site

Determination of active site in inhibitors is important to corrosion inhibition mechanism. Active sites of inhibitors can be determined with computational chemistry methods by using contour diagram of some occupied molecular orbitals, Molecular Electrostatic Potential (MEP) maps, MEP contours and Fukui functions.

#### Condensed Fukui functions

The active sites in inhibitors can be analyzed by using Fukui functions. The higher value of Fukui functions mean that the higher active and Fukui functions provide important information about inhibitors. The active sites for nucleophilic attacks, electrophilic attack and radicalic attack in molecule are related to highest  $f_k^+$  value, highest  $f_k^-$  value and highest  $f_k^0$  value, respectively. Schematic diagrams of inhibitors are represented in Fig. 1 with atomic labeling.

Fukui functions of heteroatoms which are presented in Fig.1 are calculated HF/6-31G level in water with Eqs. (10) – (12) and listed in Table 4.

According to the Table 4, nucleophilic and radicalic active sites are  $N1$  atoms for inhibitor (1) – (6). As for the electrophilic active sites,  $N2$  atom in inhibitor (1) – (6) is active site.

#### Contour diagram of some molecular orbitals

The importance of HOMO energies is explained in “Non-protonated inhibitor” section. Additionally, contour diagram of HOMO is related to active site in inhibitor. However electrons can be transferred from HOMO-1 or HOMO-2 to metal surface. If the energy differences between HOMO and HOMO-1 or HOMO-1 and HOMO-2 are small, electron may be transferred from HOMO-2, HOMO-1 or HOMO. In contour diagrams of selected molecular orbital, there are red and green lobes in different sizes. The bigger lobes mean that the highest contribution to molecular orbitals. According to the Fig. 7, HOMO electrons in inhibitor (1) – (6) are localized on imidazoline ring and lobe of  $N1$  atom on imidazoline ring is bigger than other lobes. In HOMO-1, electrons are localized on imidazoline ring and lobe on  $N1$  atom is bigger than other lobes, too. As for the HOMO-2, electrons are mainly localized on aliphatic chain and some lobes on  $N1$  atom are seen from Fig. 7. As a result,  $N1$  atom is the active sites for mentioned inhibitors. The energy differences between HOMO–HOMO-1 and HOMO-1–HOMO-2 are smaller than 2 eV. Electrons therefore can be transferred from HOMO, HOMO-1 or HOMO-2.

#### Molecular electrostatic potential (MEP) maps and contours

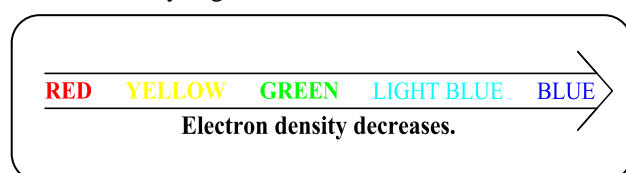
Different values of electrostatic potential at MEP map are represented by different colors which are red, yellow,

Table 4: Fukui functions of investigated inhibitors at HF/6-31G in water.

Inhibitors	Heteroatoms <sup>a</sup>	$P_k(N-1)$	$P_k(N)$	$P_k(N+1)$	$f_k^-$	$f_k^0$	$f_k^+$
Inhibitor (1)	N1	7.30708	7.65524	7.90151	0.34816	0.29721	0.24627
	N2	7.13509	7.58832	7.60973	0.45323	0.23732	0.02141
	O1	8.82835	8.82550	8.85033	-0.00285	0.01099	0.02483
Inhibitor (2)	N1	7.30707	7.64698	7.90157	0.33991	0.29725	0.25459
	N2	7.13512	7.58958	7.60969	0.45446	0.23728	0.02011
	O1	8.82835	8.83148	8.85032	0.00313	0.01098	0.01884
Inhibitor (3)	N1	7.30706	7.65268	7.90159	0.34562	0.29726	0.24891
	N2	7.13514	7.58973	7.60966	0.45459	0.23726	0.01993
	O1	8.82835	8.83243	8.85032	0.00408	0.01098	0.01789
Inhibitor (4)	N1	7.30704	7.65271	7.90163	0.34567	0.29729	0.24892
	N2	7.13518	7.58974	7.60964	0.45456	0.23723	0.01990
	O1	8.82834	8.83245	8.85033	0.00411	0.01099	0.01788
Inhibitor (5)	N1	7.30701	7.65274	7.90167	0.34573	0.29733	0.24893
	N2	7.13524	7.58973	7.60961	0.45449	0.23718	0.01988
	O1	8.82833	8.83244	8.85034	0.00411	0.01100	0.01790
Inhibitor (6)	N1	7.30697	7.64703	7.90173	0.34006	0.29738	0.25470
	N2	7.13531	7.58959	7.60958	0.45428	0.23713	0.01999
	O1	8.82831	8.83146	8.85036	0.00315	0.01102	0.01890

<sup>a</sup> These heteroatoms are represented in Scheme 1.

green, light blue and blue. According to the colors, electron density is given as follow:



The red and yellow regions in MEP map are related to electrophilic reactivity and the light blue and blue regions in MEP map is related to nucleophilic reactivity. In MEP contours, there are two colour lines which are yellow and red and these line related to positive charges and negative charges, respectively. Additionally, steric effect can be easily seen from MEP contour. MEP maps and contours are represented in Fig. 8 and Fig. 9, respectively

According to the Figs. 8 and 9, electrophilic active regions are around *N1* atom in inhibitor (1) – (6). As can be seen from MEP contour of studied inhibitors, active site is *N1* atom for inhibitor (1) – (6).

#### Protonated Inhibitors and Metal – Inhibitor Interaction

*N1* atom has been determined as active site in for mentioned inhibitors. This atom in each inhibitor therefore is protonated and optimized structure of protonated inhibitors is represented in Fig. 10. Proton affinities of investigated inhibitors are calculated by using Eq. (13) and (14) and these parameters is founded as -224.866, -224.816, -224.780, -224.793, -224.782 and -224.774 kJ/mol for inhibitor (1) – (6), respectively. According to the proton affinity values, protonation is exothermic process.

Inhibition efficiencies of investigated inhibitors are obtained towards mild steel experimentally. Percentage of iron in mild steel is about 98. Iron therefore is selected as metal in calculations. Metallic bulk causes to convergence failure in many times. Therefore, iron atom is used in calculations. Optimized structures of metal – inhibitor complexes are represented in Fig. 11 and some structural parameters for protonated inhibitors and metal – inhibitor complexes are listed in Table 5.

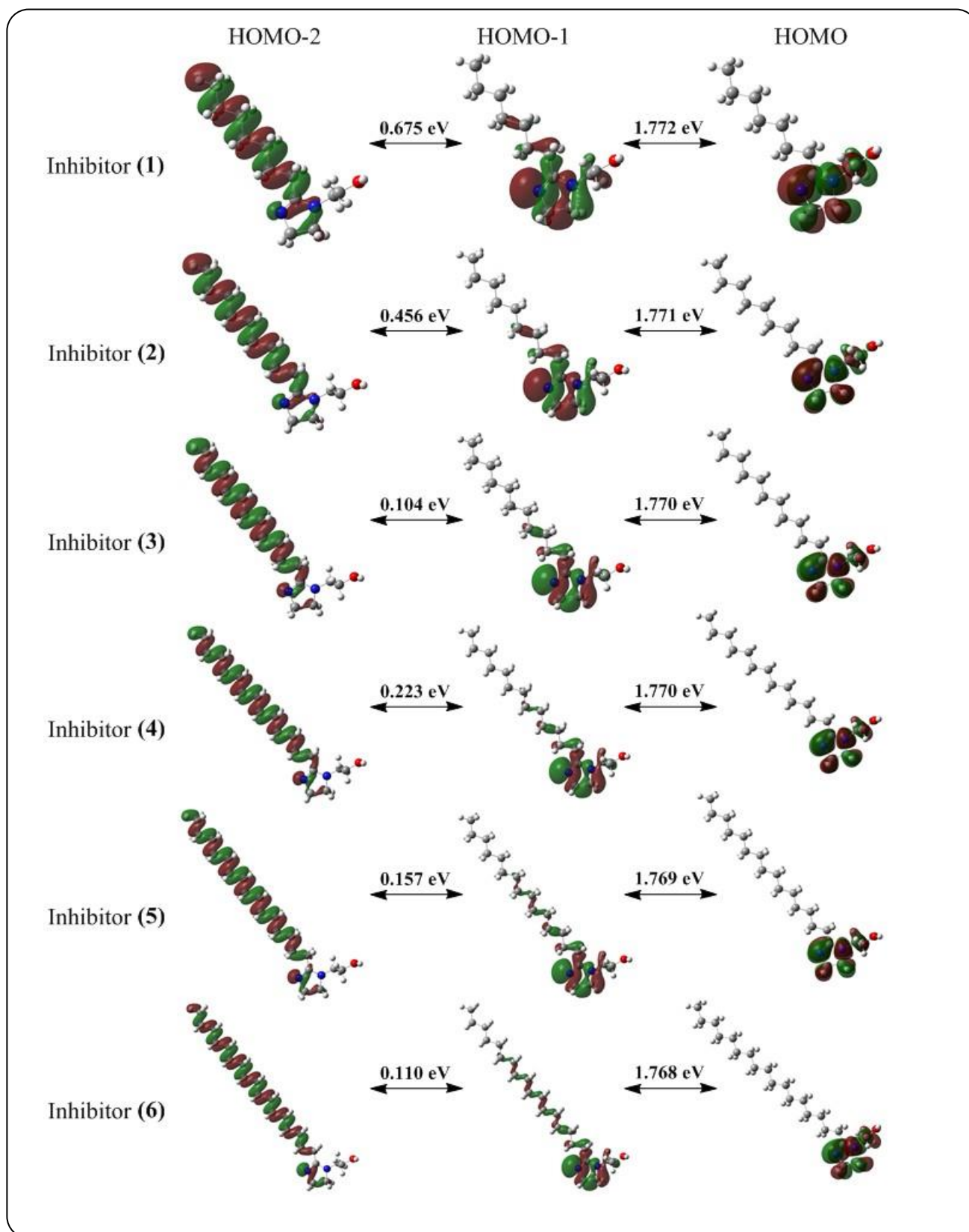
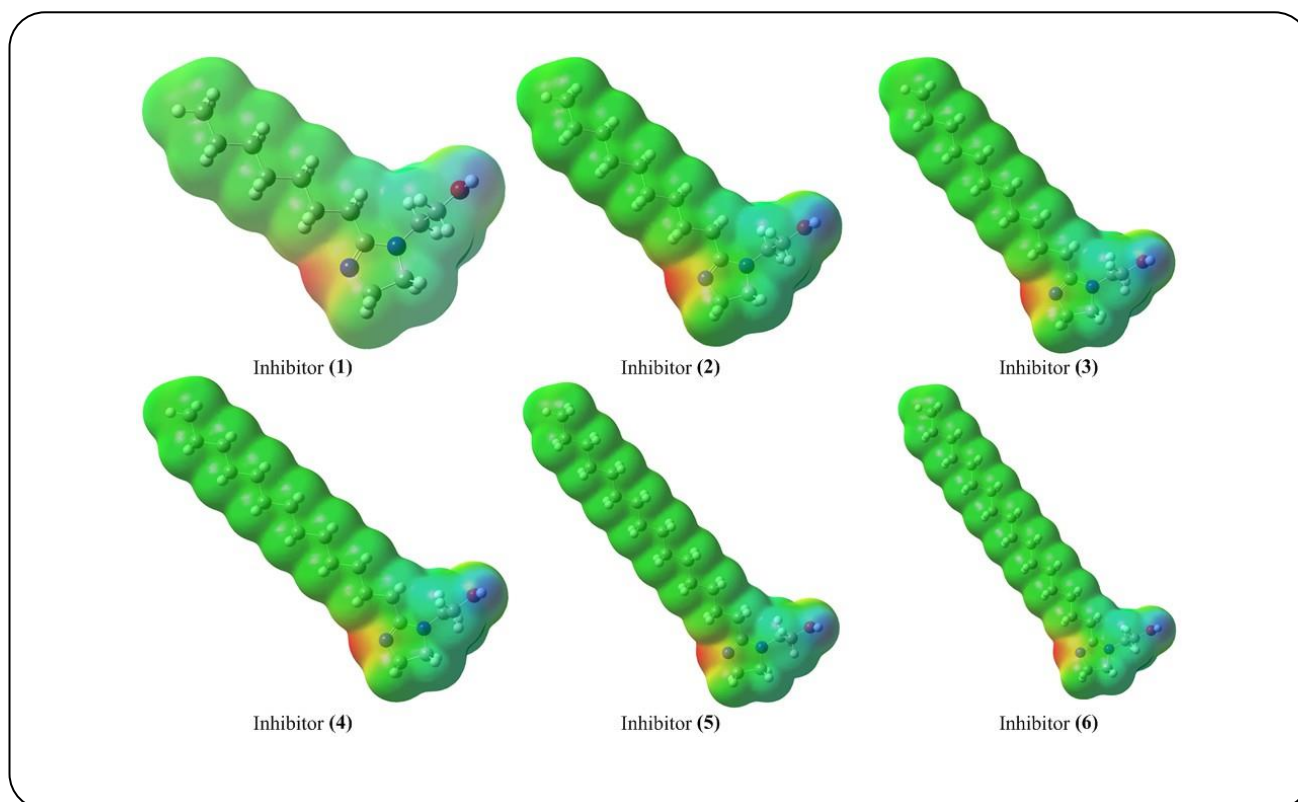
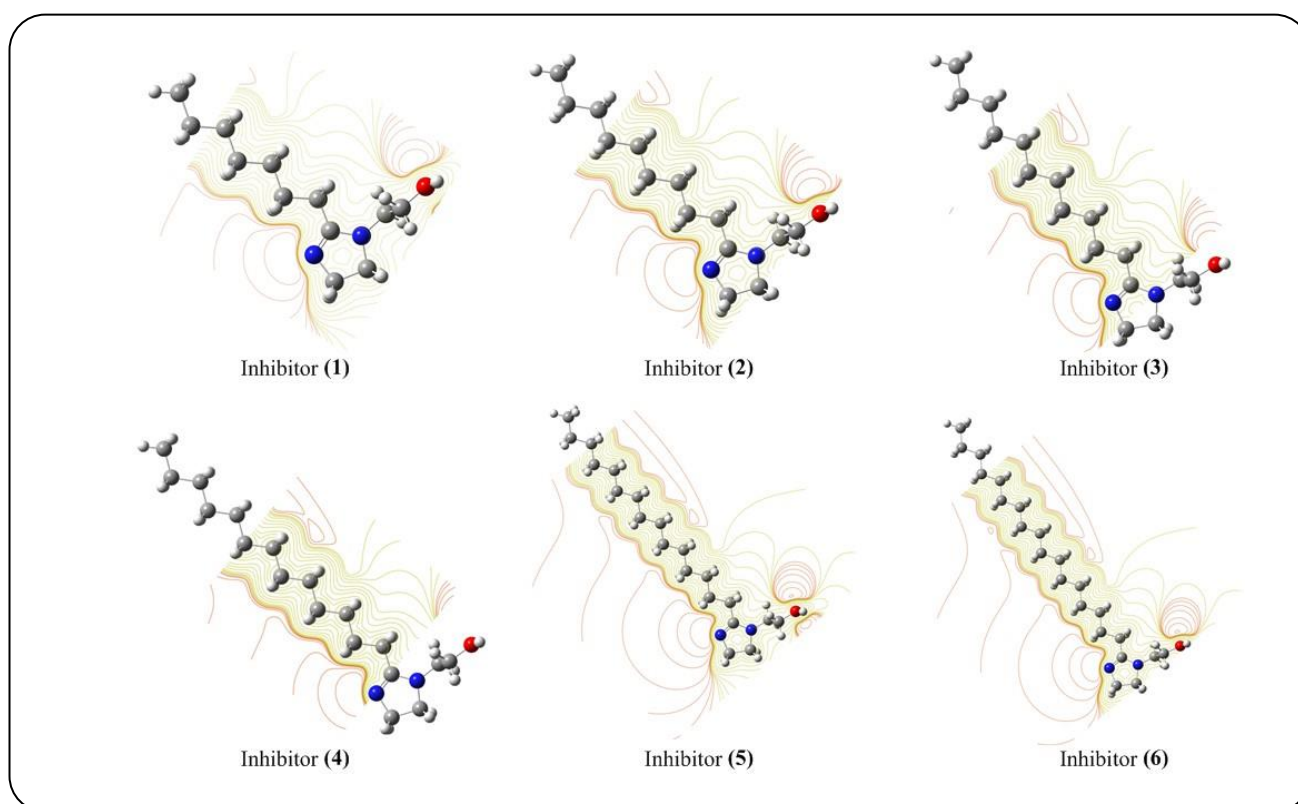


Fig. 7: Contour diagrams of HOMO, HOMO-1 and HOMO-2 of investigated inhibitors at HF method with 6-31G basis set in water.



*Fig. 8: MEP maps of investigated inhibitors at HF method with 6-31G basis set in water.*



*Fig. 9: MEP contours of investigated inhibitors at HF method with 6-31G basis set in water.*

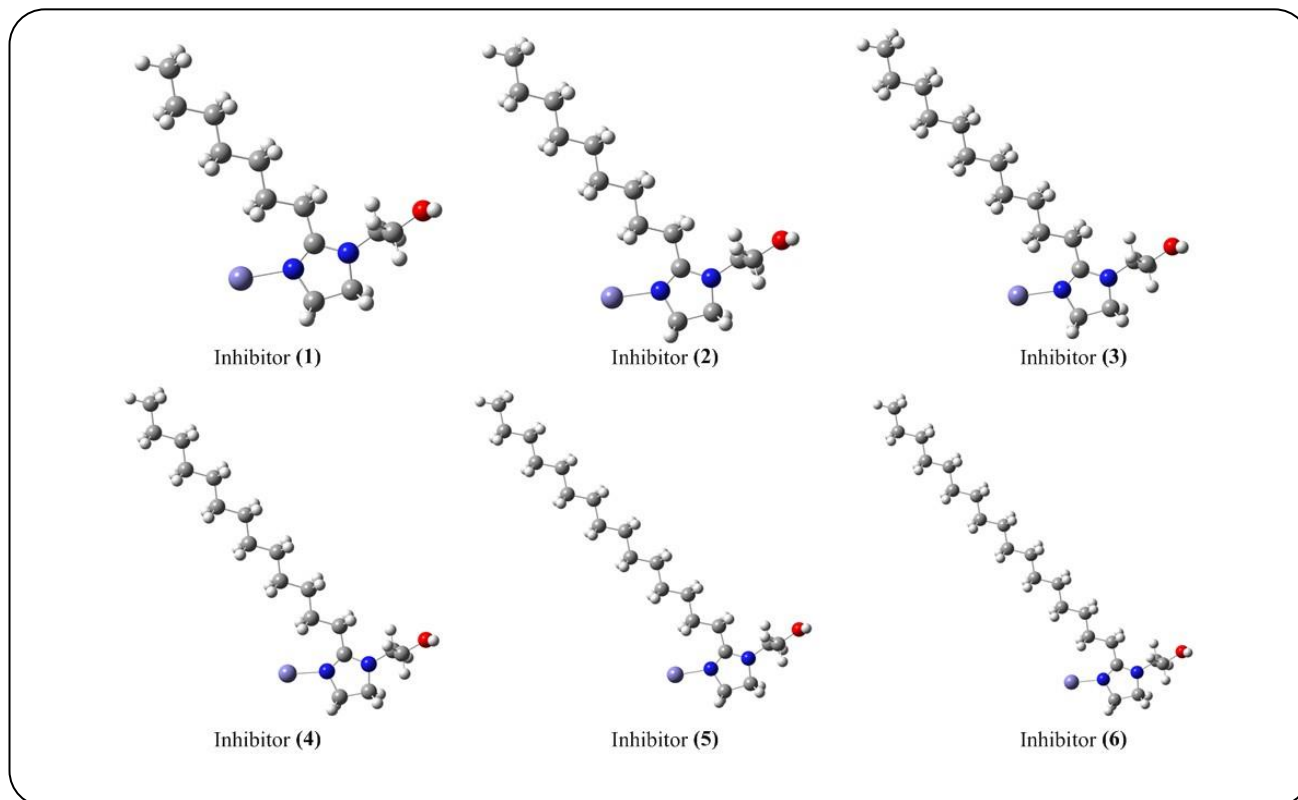


*Fig. 10: Optimized structures of protonated inhibitors at HF/6-31G level in water*

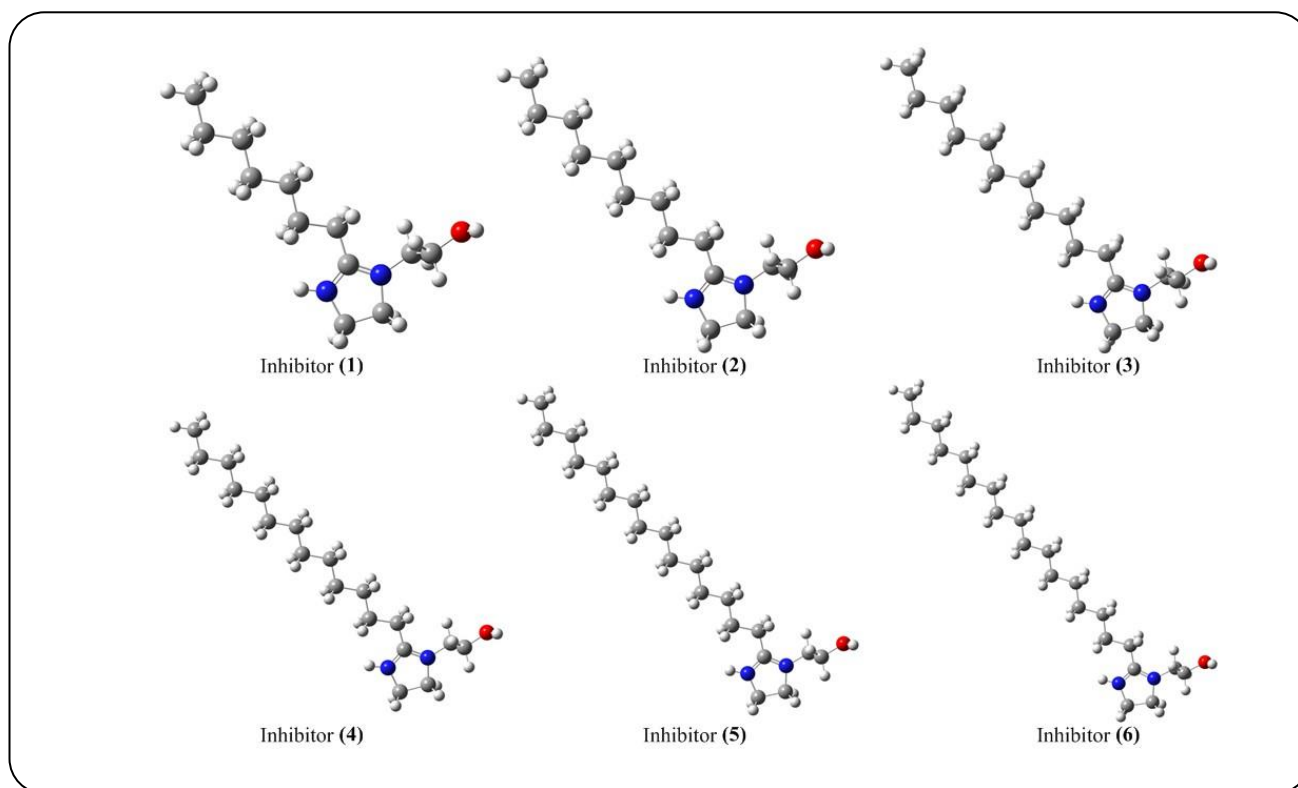


*Fig. 11: Optimized structures of metal – inhibitor complexes at HF/6-31G level in water.*

Table 5: Some structural parameters for protonated inhibitors and metal-inhibitor complexes at HF/6-31G level in water.

For protonated inhibitors								
	Bond Lengths (Å)					Bond Angles (°)		
	H – N1	N1 – C1	N1 – C1 <sup>a</sup>	C1 – N2	C1 – N2 <sup>a</sup>	H-N1-C1	N1-C1-N2	N1-C1-N2 <sup>a</sup>
Inhibitor (1)	0.99149	1.31520	1.28145	1.31991	1.37808	124.17	111.11	114.92
Inhibitor (2)	0.99146	1.31519	1.28144	1.31989	1.37800	124.15	111.11	114.93
Inhibitor (3)	0.99146	1.31521	1.28142	1.31988	1.37797	124.13	111.10	114.93
Inhibitor (4)	0.99145	1.31522	1.28141	1.31985	1.37794	124.13	111.10	114.93
Inhibitor (5)	0.99146	1.31523	1.28141	1.31985	1.37791	124.13	111.10	114.93
Inhibitor (6)	0.99146	1.31523	1.28141	1.31985	1.37788	124.13	111.10	114.93
For metal – inhibitor complexes								
	Bond Lengths (Å)					Bond Angles (°)		
	Fe – N1	N1 – C1	N1 – C1 <sup>a</sup>	C1 – N2	C1 – N2 <sup>a</sup>	Fe-N1-C1	N1-C1-N2	N1-C1-N2 <sup>a</sup>
Inhibitor (1)	2.08804	1.29706	1.28145	1.35774	1.37808	140.33	113.84	114.92
Inhibitor (2)	2.08468	1.29711	1.28144	1.35748	1.37800	140.26	113.85	114.93
Inhibitor (3)	2.08419	1.29714	1.28142	1.35742	1.37797	140.24	113.85	114.93
Inhibitor (4)	2.08414	1.29715	1.28141	1.35742	1.37794	140.26	113.85	114.93
Inhibitor (5)	2.08380	1.29716	1.28141	1.35719	1.37791	140.29	113.85	114.93
Inhibitor (6)	2.08388	1.29711	1.28141	1.35745	1.37788	140.29	113.84	114.93

<sup>a</sup> in non-protonated inhibitors

Interaction energy between metal atom and inhibitor is calculated by using Eq. (15) and these values are calculated as -32.80, -32.99, -32.98, -32.96, -32.96 and -32.96 kJ/mol for inhibitor (1) – (6), respectively. In structural parameters for protonated inhibitors, the bond length between proton and N1 atoms is close to 0.99 Å in each inhibitor. Bond lengths (N1 – C1 and C1 – N2) in protonated inhibitor are longer than in non-protonated inhibitors. This elongation is caused from the binding of proton. The angle (N1 – C1 – N2) in protonated inhibitors is more narrow than in non-protonated inhibitors. Same results in bond lengths and angles are observed in metal – inhibitor complexes. The bond length in Fe – N1 is calculated about 2.084 Å.

#### Determinations of theoretical inhibition efficiency ( $IE\%_{Theo}$ )

From all of the foregoing discussions and from Table 3 and Fig. 7, the quantum chemical parameters are in agreement with the inhibition efficiencies. The best correlation is obtained between the theoretical quantum

chemical parameters in HF/6-31G in water and the experimental corrosion inhibition efficiency. A new formula is derived to propose theoretical inhibition efficiency ( $IE\%_{Theo}$ ) by using matrix solutions. There is a relationship between the parameters and coefficient of each parameter which are calculated by using matrix solution and these coefficients do not demonstrate the general trends of inhibition efficiency. Therefore it is necessary that the result which is obtained from Eq. (16) is taken into account to interpret the theoretical inhibition efficiency of mentioned inhibitors. Eq. (16) is shown as follows:

$$IE\%_{Theo} = (624.6 \times 10^2) \times (E_{HOMO}) - \quad (16)$$

$$(-213.76 \times 10^2) \times (E_{GAP}) + (-699) \times (PA) +$$

$$(115.444 \times 10^3) \times (\sigma) + (-174.6 \times 10^1) \times (\chi) +$$

$$(609.3 \times 10^1) \times (N)$$

The above equation is derived from experimental efficiencies and theoretical results are obtained at

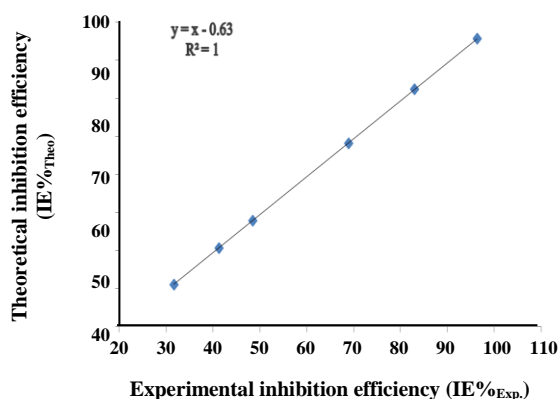


Fig. 12: Correlation between experimental (IE%<sub>Exp.</sub>) and calculated inhibition efficiency (IE%<sub>Theo.</sub>) of the studied molecules using multiple linear regression model.

HF/6-31G in water. By using Eq. (16), theoretical inhibition efficiencies are calculated as 31.07, 40.67, 47.87, 68.27, 82.37 and 95.67 for inhibitor (1), (2), (3), (4), (5) and (6), respectively. Theoretical inhibition efficiency for each inhibitor and their experimental values are subjected to correlation analyses and graph of this correlation, correlation coefficient and equation of this graph are represented in Fig. 12.

## CONCLUSIONS

The addition of imidazoline derivatives with different alkyl chain length to H<sub>2</sub>S solution reduces corrosion of steel. It was found that the ranking of the compounds should in descending order of potency be:

Inhibitor (6) > Inhibitor (5) ≈ Inhibitor (4) ≈ Inhibitor (3) > Inhibitor (2) > Inhibitor (1)

Polarization measurements demonstrate that inhibitors behaved as mixed type corrosion inhibitor by inhibiting both anodic metal dissolution and cathodic hydrogen evolution reactions. Impedance measurements indicate that with increasing inhibitor concentration, the polarization resistance ( $R_{ct}$ ) increased, while the double-layer capacitance ( $C_{dl}$ ) decreased. The high resolution AFM micrographs showed that the corrosion of steel in the solution was described by corrosion attack and the addition of inhibitors to the aggressive solutions diminished the corrosion of steel. Inhibition efficiency ranking of mentioned inhibitors were investigated by using some quantum chemical descriptor which were calculated at HF/6-31G and M062X/6-31G level in gas phase and water. The best agreement are obtained

at HF/6-31G level in water with experimental results. Therefore HF/6-31G level is taken into account for other calculations. Active sites of mentioned inhibitors were investigated by using Fukui functions, contour diagram of HOMO, MEP map and MEP contour. N1 atom is determined as active site for inhibitor (1) – (6). Proton affinity and interaction energies between metal atom and inhibitor are investigated. For determining the theoretical inhibition efficiency of investigated inhibitors, a new formula for these type inhibitors was derived by using experimental inhibition efficiencies and quantum chemical parameters at HF/6-31G level in water.

## Acknowledgments

The authors would like to acknowledge to their corresponding universities. We are grateful to the Iranian Offshore Oil Company (IOOC) of National Iranian Oil Company (NIOC) for financial supports.

Received : Nov. 29, 2015 ; Accepted : Jan. 1, 2017

## REFERENCES

- [1] Feng Z., Marks C.R., Barkatt A., [The Internal Oxidation of Ternary Alloys I: The Single Oxidation of the Most-Reactive Component Under Low Oxidant Pressures](#), *Oxid. Met.*, **60**(5-6): 347-370 (2003).
- [2] Atkinson J. T. N., Vandrofflear H., ["Corrosion and Its control"](#), Houston, Texas: NACE, 1-5 (1985).
- [3] Uhlig H. H., Revie R.W., ["Corrosion and Corrosion Control"](#), New York: Wiley & Sons, Inc., 263-277 (1985).
- [4] Jafari H., Danaee I., Eskandari H., RashvandAvei M., [Electrochemical and Theoretical Studies of Adsorption and Corrosion Inhibition of N,N'-Bis\(2-hydroxyethoxyacetophenone\) -2,2- dimethyl-1,2-propanediimine on Low Carbon Steel \(API 5L Grade B\) in Acidic Solution](#), *Ind. Eng. Chem. Res.*, **52**(20): 6617–6632 (2013).
- [5] Jong Kwon P., Noh Hee J., [Corrosion Inhibition Effect of Ester Containing Cationic Gemini Surfactants on Low Carbon Steel](#), *Iran. J. Chem. Chem. Eng. (IJCCE)*, **35** (1): 85-93 (2016).
- [6] Jafari H., Danaee I., Eskandari H., RashvandAvei M., [Combined Computational and Experimental Study on the Adsorption and Inhibition Effects of N<sub>2</sub>O<sub>2</sub> Schiff Base on the Corrosion of API 5L Grade B Steel in 1 mol/L HCl](#), *J. Mater. Sci. Technol.*, **30**(3): 239-252 (2014).



- [7] Liu F.G., Du M., Zhang J., Qiu M., [Electrochemical Behavior of Q235 Steel in Saltwater Saturated with Carbon Dioxide Based on New Imidazoline Derivative Inhibitor](#), *Corros. Sci.*, **51**(1): 102-109 (2009).
- [8] Okafor P.C., Liu X., Zheng Y.G., [Corrosion inhibition of Mild steel by Ethylamino Imidazoline Derivative in CO<sub>2</sub>-Saturated Solution](#), *Corros. Sci.*, **51**(4): 761-768 (2009).
- [9] Jafari H., Danaee I., Eskandari H., RashvandAvei M., [Electrochemical and Quantum Chemical Studies of N,N'-bis\(4-hydroxybenzaldehyde\)-2,2-Dimethylpropanediimine Schiff Base as Corrosion Inhibitor for Low Carbon Steel in HCl Solution](#), *J. Environ. Sci. Heal. A.*, **48**(13): 1628-1641 (2013).
- [10] Abderrahim K., Abderrahmane S., Millet J., [Inhibition of Copper Corrosion by Ethanolamine in 100 ppm NaCl](#), *Iran. J. Chem. Chem. Eng. (IJCCE)*, **35**(4): 89-98 (2016).
- [11] Danaee I., Gholami M., RashvandAvei M., Maddahy M.H., [Quantum Chemical and Experimental Investigations on Inhibitory Behavior of Amino-Imino Tautomeric Equilibrium of 2-Aminobenzothiazole on Steel Corrosion in H<sub>2</sub>SO<sub>4</sub> Solution](#), *J. Ind. Eng. Chem.*, **26**(25): 81-94 (2015).
- [12] Anastas P.T., "Green Chemistry", John Wiley & Sons, Inc., 3 335-340 (2014).
- [13] Roy Dennington, Todd Keith, John Millam, "Introduction to GaussView and Gaussian, Version 5", Semiche Inc., Shawnee Mission, KS, (2009).
- [14] [Gaussian 09](#), RevisionD.01, M.J. Frisch, G. W. Trucks, H. B. Schlegel, G. E. Scuseria, M. A. Robb, J.R. Cheeseman, G. Scalmani, V. Barone, B. Mennucci, G. A. Petersson, H. Nakatsuji, M. Caricato, X. Li, H. P. Hratchian, A. F. Izmaylov, J. Bloino, G. Zheng, J. L. Sonnenberg, M. Hada, M. Ehara, K. Toyota, R. Fukuda, J. Hasegawa, M. Ishida, T. Nakajima, Y. Honda, O. Kitao, H. Nakai, T. Vreven, J. A. Montgomery, Jr., J. E. Peralta, F. Ogliaro, M. Bearpark, J. J. Heyd, E. Brothers, K. N. Kudin, V. N. Staroverov, R. Kobayashi, J. Normand, K. Raghavachari, A. Rendell, J. C. Burant, S. S. Iyengar, J. Tomasi, M. Cossi, N. Rega, J. M. Millam, M. Klene, J. E. Knox, J. B. Cross, V. Bakken, C. Adamo, J. Jaramillo, R. Gomperts, R. E. Stratmann, O. Yazyev, A. J. Austin, R. Cammi, C. Pomelli, J. W. Ochterski, R. L. Martin, K. Morokuma, V. G. Zakrzewski, G. A. Voth, P. Salvador, J. J. Dannenberg, S. Dapprich, A. D. Daniels, Ö. Farkas, J. B. Foresman, J. V. Ortiz, J. Cioslowski, and D. J. Fox, Gaussian, Inc., Wallingford CT, (2009).
- [15] PerkinElmer, "ChemBioDraw Ultra Version" (13.0.0.3015), CambridgeSoft Waltham, MA, USA (2012).
- [16] Yıldız R., [An Electrochemical and Theoretical Evaluation of 4,6-diamino-2-pyrimidinethiol as a Corrosion Inhibitor for Mild Steel in HCl Solutions](#), *Corros. Sci.*, **90**: 544 – 553 (2015).
- [17] Zhang K., Xu B., Yang W., Yin X., Liu Y., Chen Y., [Halogen-Substituted Imidazoline Derivatives as Corrosion Inhibitors for Mild steel in Hydrochloric Acid Solution](#), *Corros. Sci.*, **90** : 284 – 295 (2015).
- [18] Guo L., Zhu Sh., Zhang Sh., He Q., Li W., [Theoretical Studies of Three Triazole Derivatives as Corrosion Inhibitors for Mild Steel in Acidic Medium](#), *Corros. Sci.*, **87** : 366 – 375 (2014).
- [19] Mert B.D., Yüce A.O., Kardas G., Yazıcı B., [Inhibition Effect of 2-amino-4-methylpyridine on Mild Steel Corrosion: Experimental and Theoretical Investigation](#), *Corros. Sci.*, **85**: 287 – 295 (2014).
- [20] Obot I.B., Gasem Z.M., [Theoretical Evaluation of Corrosion Inhibition Performance of Some Pyrazine Derivatives](#), *Corros. Sci.*, **83**: 359 – 366 (2014).
- [21] Sayin K. Karakaş D., [Quantum Chemical Studies on the Some Inorganic Corrosion Inhibitors](#), *Corros. Sci.*, **77**: 37 – 45 (2013).
- [22] Karakus N., Sayin K., [The Investigation of Corrosion Inhibition Efficiency on Some Benzaldehyde Thiosemicarbazones and Their Thiole Tautomers: Computational Study](#), *J Taiwan. Inst. Chem. Eng.*, **48**: 95-102 (2014).
- [23] Mohsenifar F, Jafari H, Sayin K, [Investigation of Thermodynamic Parameters for Steel Corrosion in Acidic Solution in the Presence of N, N'-bis \(phloroacetophenone\)-1, 2 propanediamine](#), *J. Bio. Tribo. Corros.*, **2**(1): 1-13 (2016).
- [24] Zarrouk A., Hammouti B., Lakhlifi T., Traisnel M., Vezin H., Bentiss F., [New 1H-pyrrole-2,5-dione Derivatives as Efficient Organic Inhibitors of Carbon Steel Corrosion in Hydrochloric Acid Medium: Electrochemical, XPS and DFT Studies](#), *Corros. Sci.* **90**: 572 – 584 (2015).

- [25] Abd El-Lateef H.M., Experimental and Computational Investigation on the Corrosion Inhibition Characteristics of Mild Steel by Some Novel Synthesized Imines in Hydrochloric Acid Solutions, *Corros. Sci.*, **92**: 104-117 (2015).
- [26] Kaya S., Kaya C., A New Equation Based on Ionization Energies and Electron Affinities of Atoms for Calculating of Group Electronegativity, *Comput. Theor. Chem.*, **1052** (15): 42 – 46 (2015).
- [27] Wazzan N.A., DFT Calculations of Thiosemicarbazide, Arylisothiocyanates, and 1-aryl-2,5-dithiohydrazodicarbonamides as Corrosion Inhibitors of Copper in an Aqueous Chloride Solution, *J. Ind. Eng. Chem.*, **26**(25): 291-308 (2015).
- [28] Fujioka E., Nishihara H., Aramaki K., The Inhibition of Pit Nucleation and Growth on the Passive Surface of Iron in a Borate Buffer Solution Containing Cl by Oxidizing Inhibitors, *Corros. Sci.*, **38**(11): 1915 – 1933 (1996).
- [29] Kiyooka S., Kaneno D., Fujiyama R., Parr's Index to Describe both Electrophilicity and Nucleophilicity, *Tetrahedron. Lett.* 54(4): 339 – 342 (2013).
- [30] Jafari H., Akbarzade K., Danaee I., Corrosion Inhibition of Carbon Steel Immersed in a 1M HCl Solution Using Benzothiazole Derivatives, *Arab. J. Chem.*, (2014).  
<https://doi.org/10.1016/j.arabjc.2014.11.018>.
- [31] Ashassi-Sorkhabi H., Shaabani B., Seifzadeh D., Corrosion Inhibition of Mild Steel by Some Schiff Base Compounds in Hydrochloric Acid, *Appl. Surf. Sci.*, **239** (2): 154–164 (2005).
- [32] Sayin K, Jafari H, Mohsenifar F, Effect of Pyridyl on Adsorption Behavior and Corrosion Inhibition of Aminotriazole, *J. Taiwan Instit. Chem. Engin.*, **68**: 431-439 (2016).
- [33] Chetouani A., Aouniti A., Hammouti B., Benchat N., Benhadda T., Kertit S., Corrosion Inhibitors for Iron in Hydrochloride Acid Solution by Newly Synthesised Pyridazine Derivatives, *Corros. Sci.*, **45**(8): 1675–1684 (2003).
- [34] Emeregül K.C., Hayval M., Studies on the Effect of a Newly Synthesized Schiff Base Compound from Phenazone and Vanillin on the Corrosion of Steel in 2 M HCl, *Corros. Sci.*, **48**(4): 797–812 (2006).
- [35] Jafari H., Danaee I., Eskandari H., Inhibitive Action of Novel Schiff Base Towards Corrosion of API 5L Carbon Steel in 1 M Hydrochloric Acid Solutions, *Trans. Indian Inst. Met.*, 68(5): 729–739 (2015).
- [36] Olivares O., Likhanova N.V., Gomez B. J., Navarrete B., Llanos-Serrano M. E., Arce E., Hallen J.M., Electrochemical and XPS Studies of Decylamides of Alphaamino Acids Adsorption on Carbon Steel in Acidic Environment, *Appl. Surf. Sci.*, **252**: 2894–2909 (2006).
- [37] Abdel Rehim S.S., Hazzazi O.A., Amin M.A., Khaled K.F., On the Corrosion Inhibition of Low Carbon Steel in Concentrated Sulphuric Acid Solutions. Part I: Chemical and Electrochemical (AC and DC) Studies, *Corros. Sci.*, **50** (8): 2258–2271 (2008).
- [38] Saleh M.M., Atia A.A., Effects of Structure of the Ionic Head of Cationic Surfactant on Its Inhibition of Acid Corrosion of Mild Steel, *J. Appl. Electrochem.*, **36**(8): 899-905 (2006).
- [39] Jafari H, Sayin K., Electrochemical and Theoretical Studies of Adsorption and Corrosion Inhibition of Aniline Violet Compound on Carbon Steel in Acidic Solution, *J. Taiwan Instit. Chem. Engin.*, **56**: 181-190 (2015).
- [40]. Emregül K.C., Atakol O., Corrosion Inhibition of Mild Steel with Schiff Base Compounds in 1 M HCl, *Mater. Chem. Phys.* **82**(1): 188–193 (2003).
- [41] Li X.H., Deng S.D., Fu H., Inhibition by Jasminum Nudiflorum Lindl. Leaves Extract of the Corrosion of Cold Rolled Steel in Hydrochloric Acid Solution, *J. Appl. Electrochem.*, **40**(9): 1641–1649 (2010).
- [42] Larabi L., Harek Y., Traianel M., Mansri A., Synergistic Influence of Poly(4-vinylpyridine) and Potassium Iodide on Inhibition of Corrosion of Mild Steel in 1 M HCl, *J. Appl. Electrochem.*, **34** (8): 833–839 (2004).
- [43] Jafari H., Sayin K., Sulfur Containing Compounds as Corrosion Inhibitors for Mild Steel in Hydrochloric Acid Solution, *Trans. Indian Inst. Met.*, **69**(3): 805–815 (2016).
- [44] Shih H., Mansfeld F., A Fitting Procedure for Impedance Data of Systems with Very Low Corrosion Rates, *Corros. Sci.*, **29**(10): 1235–1240 (1989).

- [45] Martinez S., Metikoš-Huković M. , [A Nonlinear Kinetic Model Introduced for the Corrosion Inhibitive Properties of Some Organic Inhibitors](#), *J. Appl. Electrochem.*, **33**(12): 1137–1142 (2003).
- [46] Jafari H., Akbarzade K., [Effect of Concentration and Temperature on Carbon Steel Corrosion Inhibition](#), *J. Bio. Tribo. Corros.*, **3**(8): 8–14 (2017).
- [47] Danaee I., Noori S., [Kinetics of the Hydrogen Evolution Reaction on NiMn Graphite Modified Electrode](#), *Int. J. Hydrogen Energ.*, **36**(19): 12102–12111 (2011).
- [48] Aramaki, K. Hagiwara M., Nishihara H., [A Study on the Oxidative-Addition Reaction of Benzyl Compounds in Sulphuric Acid and Its Relation to Corrosion Inhibition](#), *Corros. Sci.*, **28** (4): 343-352 (1988).